SCIENTIFIC PAPERS
OF THE UNIVERSITY OF PARDUBICE
Series A
Faculty of Chemical Technology
19 (2013)

APPLICATION OF POLYANILINE DISPERSIONS BY MEANS OF SCREEN PRINTING

Markéta DRŽKOVÁ[1a], Nikola PEŘINKA[a], Milena HAJNÁ[b], Marie KAPLANOVÁ[a] and Jaroslav STEJSKAL[b]
[a]Department of Graphic Arts and Photophysics,
The University of Pardubice, CZ–532 10 Pardubice,
[b]Institute of Macromolecular Chemistry, Academy of Sciences of the Czech Republic, CZ–162 06 Prague

Received September 30, 2013

In the recent time, the printing of functional substances (e.g., conducting polymers, metal-particle composites, carbon black and graphene based materials, etc.) has become of large importance. The main reason is the establishment of so-called printed electronics, where such substances are applied and later form functional electronic devices (e.g., sensors, displays, photovoltaic cells, transistors, etc.). Polyaniline has been reported to be a very versatile conducting polymer. Therefore, its application in a form of functional coatings and thin layers is desired. Polyaniline can be prepared in the presence of water-soluble polymeric stabilizers [e.g., poly(N-vinylpyrrolidone)], so that stable colloidal dispersions are obtained after the synthesis based on the oxidation of aniline with ammonium peroxydisulfate. These dispersions must be further adjusted for the needs of printing. This work is focused on the application of polyaniline-based dispersions

[1] To whom correspondence should be addressed.

by means of screen-printing method. A screen-printable formulation of polyaniline-based dispersion was prepared and printed on Melinex® ST504 poly(ethylene terephthalate) substrate. The quality and functionality of the prepared layers was studied by means of common methods (electrical resistance measurement, profilometry, optical microscopy with image analysis, optical spectroscopy). The prepared polyaniline films were examined also by means of photoacoustics, where changes in the subsurface structure and thickness of the polyaniline layers could be observed. The influence of the printing parameters as well as the components of the prepared formulations on the resulting quality and functionality was investigated.

Introduction

The application of organic compounds in electronics by means of printing is constantly growing nowadays [1]. A very promising area of novel organic materials is the conducting polymers, which are currently mainly represented by polythiophenes (e.g., poly(3,4-ethylene-dioxythiophene) poly(styrenesulfonate), i.e., PEDOT:PSS) [2,3] and polyanilines (PANI) [4,5]. The polyanilines and their composites have been intensively studied in the past few decades, and their application in electronics has been intended; the interesting applications in the present time include fabrication of sensors, photovoltaic cells, actuators, electrodes, etc. [6-9]. Most of the PANI layers for the electronic devices are currently prepared by means of common laboratory methods, or printed by ink-jet [5,6,10]. One of the other possible methods for the application of PANI is the screen printing technique, which may be, in accordance with the principle of this method, used for the fabrication of thick structured films in flexible organic electronic devices. The main advantage of screen printing is the possibility of large area industrial fabrication. The dispersions of PANI are well suited for screen printing technique. The reason is the fact that they can form stable liquids with higher viscosity. Few years ago, the screen printing of PANI ink systems based on organic solvents was published [11]. Because there is still a lack of publications referring to the screen printing of PANI water-based systems, this work is focused on this area. The poly(*N*-vinylpyrrolidone) (PVP) stabilized PANI water based dispersion [12] was chosen as the suitable material, and the possibility of its application by means of the screen printing has been recently verified [13]. The search for the optimum printing conditions and the control of PANI film properties is essential for desired electronic applications. The main purpose of this present work was to investigate the influence of layer thickness and morphology resulting from varied printing parameters on the performance and properties of the prepared PANI/PVP conducting layers.

Experimental

The colloidal PANI dispersion was prepared by the oxidative polymerization of aniline in aqueous medium. The oxidation of 0.20 M aniline hydrochloride was performed with 0.25 M ammonium peroxydisulfate ($(NH_4)_2S_2O_8$) in the presence of 2 wt. % PVP stabilizer (Fluka, Switzerland, type K90, mol. wt. 360,000) [12]. After the preparation, the dispersion was dialyzed against 0.2 M hydrochloric acid to remove low-molecular-weight reaction residues and by-products, and thickened by evaporation of a part of water in one or two steps. The final volumes of dispersions were 35.5 % and 12 % of the original volume, respectively.

Square samples (1.5 cm × 1.5 cm) of this PANI-based dispersion were printed on Melinex® ST504 poly(ethylene terephthalate) substrate by means of semiautomatic screen-printing machine at laboratory conditions. To achieve differing thicknesses and morphologies of layers, both the formulation of PANI-based dispersion and parameters of printing and drying were varied. The dispersion was modified to a screen-printable formulation by addition of deionised water, ethanol (EtOH) or deionised water with either butan-2-ol (BuOH) or surfactant (an anionic type, sodium 1,4-bis(2-ethylhexoxy)-1,4-dioxobutane-2-sulfonate, AOT). For the printing, mesh densities of 77, 120 or 165 1 cm^{-1} were used and either 1 layer or 4 layers wet-on-wet were printed. The printed samples were left to dry at laboratory temperature or dried in a hot-air oven either for 10 minutes at the temperature of 100 °C or for 5 minutes at 130 °C.

The surface resistance of the printed layers of PANI dispersions was studied by means of the two point probe. The contacts were prepared using conducting carbon paste for elimination of the contact resistance. The thickness and the roughness parameter (*Ra*) of the prepared layers were estimated by means of stylus profiler Veeco Dektak 150. For the study, a set of six different samples was chosen (Table I).

The morphology of the layers was studied by optical microscopy with optical microscope Bresser Erudit DLX and microscope camera Bresser MikroCam 5.0 MP. For image analysis of printed samples, microscope images with the size of 2592×1944 pixels were captured and cut to the size of 800×600 pixels. Fractal spectra of these images were determined using a box-counting method by means of the software HarFa (Harmonic and Fractal Image Analyzer [14]) using the procedure described in [15]. Fractal spectrum is the dependence of the fractal dimension on the thresholding limit *GL* (Grey Level, 0-255) for segmentation into binary black-and-white images. The fractal dimension D_{BW}, which characterizes the complexity of the interface between black and white areas of the image, was analysed.

The optical transmission spectroscopic measurements of printed samples were carried out on the spectrophotometer SPECORD 210 in the range from 350 to 1100 nm. The measured spectra were corrected by subtraction of

absorbance of the unprinted substrate.

For photoacoustic measurements, the circular samples with the diameter of 10 mm were cut from the sheet and fixed on the poly(methyl methacrylate) backing using a thin layer of medicinal white oil (MBO 46, STN 65 7310). The samples were placed to the front-detection cylindrical photoacoustic cell with the 1/2" condenser microphone (Brüel & Kjaer, type 4137). As the excitation source for modulation frequency domain measurements, the externally modulated diode pumped solid-state laser modules emitting at 473 nm (Photop Suwtech, DPBL 9020) and 655 nm (Laser Components, Flexpoint Minilaser FP 65/20ADF AV) were used, and their intensity was modulated with acoustic frequencies between 10 Hz and 1 or 5 kHz, respectively. For photoacoustic spectroscopy, the monochromator output (Jobin Yvon, Triax 190 with Osram 450 W Xe lamp) modulated at 8.5 Hz by mechanical chopper SR540 (Stanford Research Systems) was used. The detected photoacoustic signal was pre-amplified and fed to the digital signal processing lock-in amplifier SR830 (Stanford Research Systems), which was also used for the control of modulation of each of the three excitation sources. As a reference sample for signal normalization, the polypropylene foil with thin gold layer deposited by evaporation in high vacuum was used in the case of measurements in modulation frequency domain, and carbon black in the case of photoacoustic spectra measurements.

Table I Printed samples of PANI-based dispersion and their parameters

Sample		S1	S2	S3	S4	S5	S6
Thickening steps		1	1	2	2	2	2
Additives, wt. %	H_2O	-	35	57	57	57	57
	EtOH	70	-	-	-	-	-
	BuOH	-	15	-	-	-	-
	AOT	-	-	-	-	0.1	-
Mesh density, 1 cm^{-1}		120	120	77	165	165	77
Number of layers		1	1	1	1	4	4
Drying, °C (min)		25	130 (5)	100 (10)	100 (10)	25	25
Thickness, µm		0.35	2.5	5.19	1.99	1.33	2.99
Roughness (*Ra*), µm		0.10	0.56	1.53	0.40	0.36	0.64
Surface resistance MS sq^{-1}		>200	1.6	1.1	1.9	7.9	0.45
Specific conductivity, mS cm^{-1}		-	2.5	1.8	2.6	1.0	7.4

Results and Discussion

Thickness and Roughness

The thickness of the prepared samples ranged from 350 nm to 5.2 µm depending on the concentration of additives in each sample, as well as on the used mesh density and number of the printed layers (see Table I). As it is obvious from Table I, to decrease the layer thickness, a higher percentage of solvent additives (e.g., EtOH) or higher mesh densities should be taken. The increased number of the layers printed wet-on-wet also rather decreases the resulting layers thickness, which is related to the increased homogeneity of the layer. The roughness parameter *Ra* is approximately proportional to the thickness (Fig. 1). The values of *Ra* for the samples S2, S4 and S6 seem to be slightly lower than would correspond to the course of linear approximation for other three samples, however, no relation to the parameters of their preparation was found.

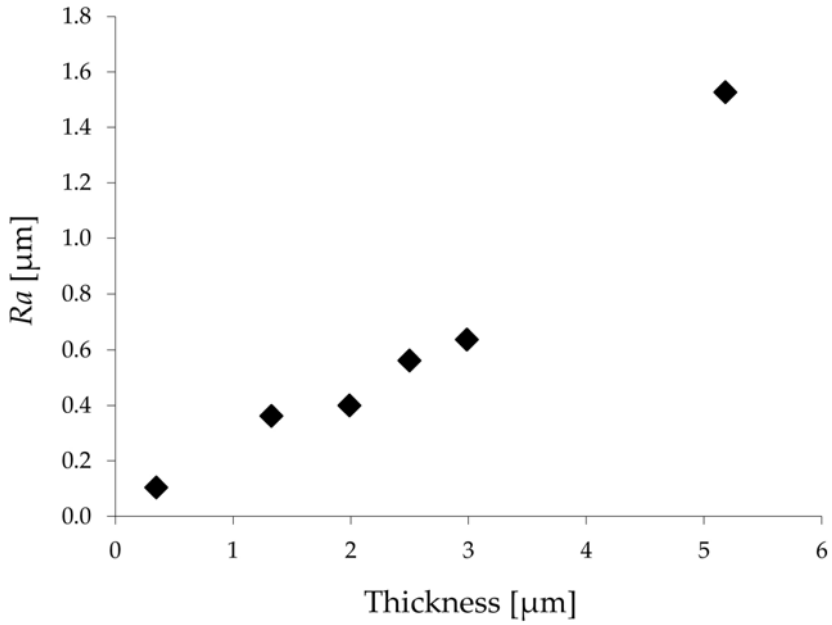

Fig. 1 Correlation between the roughness parameter *Ra* and the thickness

Electrical Conductivity

The prepared layers of PANI had relatively similar values of specific conductivity (except for sample S1, see Table I). The specific conductivity of sample S1 could not be estimated due to the fact that the surface resistance of this sample was higher than the measuring limit of the used measuring device. The values of the specific conductivity of other samples slightly varied depending on the set printing conditions. The change in the drying temperature did not show any significant im-

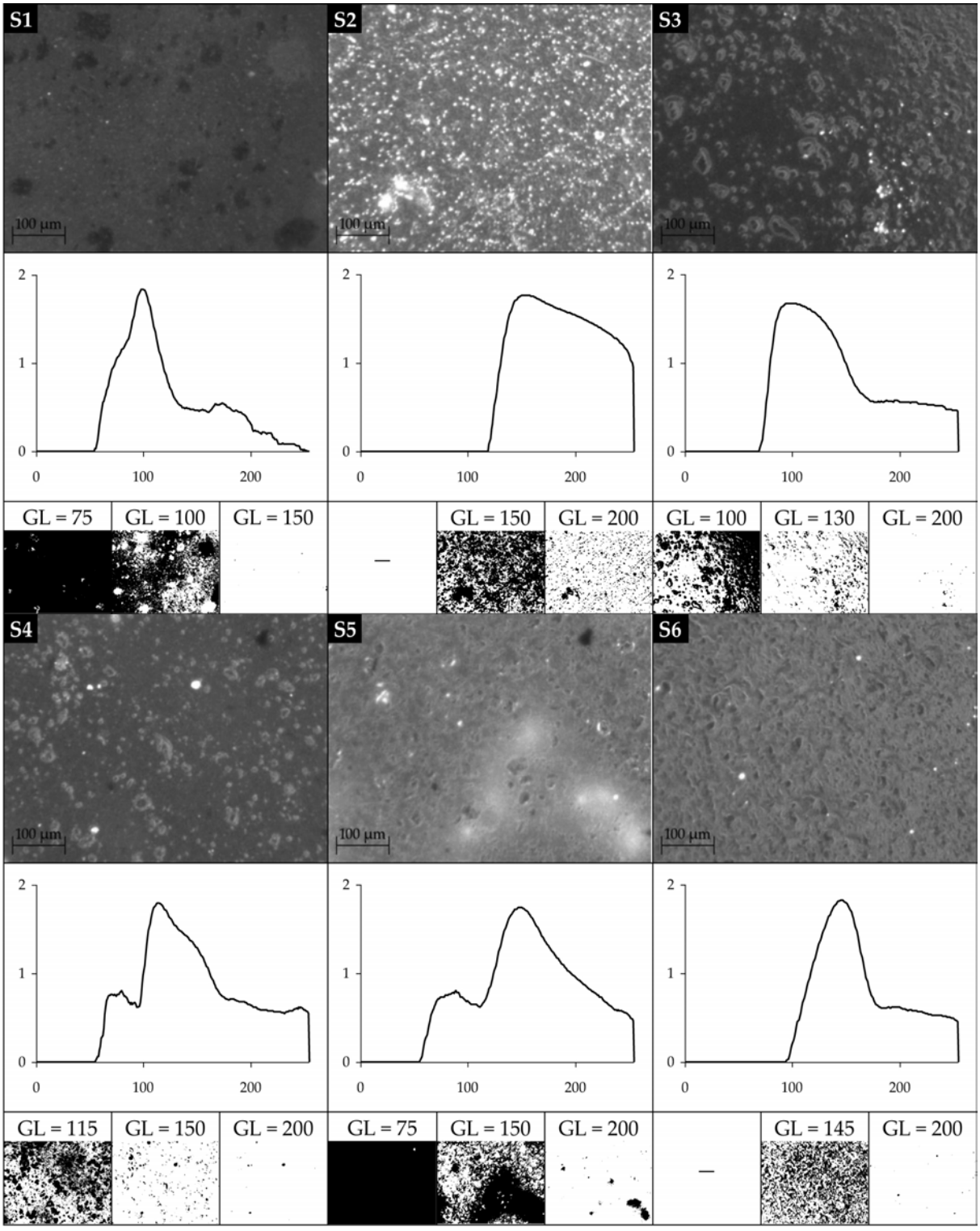

Fig. 2 Examples of captured images of printed samples of PANI-based dispersion together with their fractal spectra and corresponding bitmaps segmented at GL representing the local maxima or shoulders in fractal spectra

pact on the resulting conductivity of the prepared layers. The use of BuOH in sample S2 led to better results than addition of EtOH to sample S1. In the case of sample S5, the addition of the surfactant AOT and four times repeated printing

helped to decrease the surface roughness of the sample; however, the resulting specific conductivity was lower than that of sample S4. The highest specific conductivity was approx. 7.5 mS cm^{-1} for sample S6, and was achieved with the mesh density of 77 1 cm^{-1} and four times repeated printing.

Image Analysis

In fractal spectra of printed samples evaluated from images captured at constant conditions, the position of the maximum is the measure of dominant grey level and decreases for darker prints, whereas the width of the peak is related to the structure [15]. A more homogeneous sample results in a fractal spectrum with fewer grey levels exhibiting fractal structure, i.e., with DBW > 0 [16]. The complexity of the spectrum increases with the decrease of overall homogeneity as well as with the occurrence of various local defects [15]. In the present study, it was not possible to compare absolute positions of peak maxima and widths of the peaks in fractal spectra of individual samples, because the lighting conditions during the image capturing had to be changed. Therefore, the evaluation was based on the visual inspection and qualitative analysis of fractal spectra (Fig. 2). The highest layer uniformity was observed in the case of the best conducting sample S6. In fractal spectra, the main peak is given by the prevailing layer structure regardless of the local defects. Pinholes were observed in all samples; when they are present in a small number, they appear in the fractal spectra as a plateau with DBW around 0.5 at higher values of GL. A large number of various holes in sample S2 and local areas with lower thickness in sample S5 are also reflected in the right part of fractal spectra and cause the gradual transition into the main peak. Larger agglomerates appear as a left shoulder of the main peak, when they are flat and dark (S1); more plastic agglomerates at a higher concentration contribute to the main peak and cause its asymmetry (S3 and S4). The small peak around GL = 75 (S4 and S5) aroused due to the impurity present in the image and should be neglected.

Optical and Photoacoustic Spectra

As expected, it was practically impossible to measure optical transmission spectra for the samples with higher thickness (approximately above 2.5 μm), as even in the less-absorbing wavelength regions the transmission was below 1 %. In the case of photoacoustic spectroscopy, the amplitude is proportional to the light absorbed in the sample; therefore, the signal-to-noise (S/N) ratio generally increases with increasing sample thickness, opposite to optical transmission spectroscopy. As shown in Fig. 3 depicting normalized photoacoustic spectra, the spectral saturation

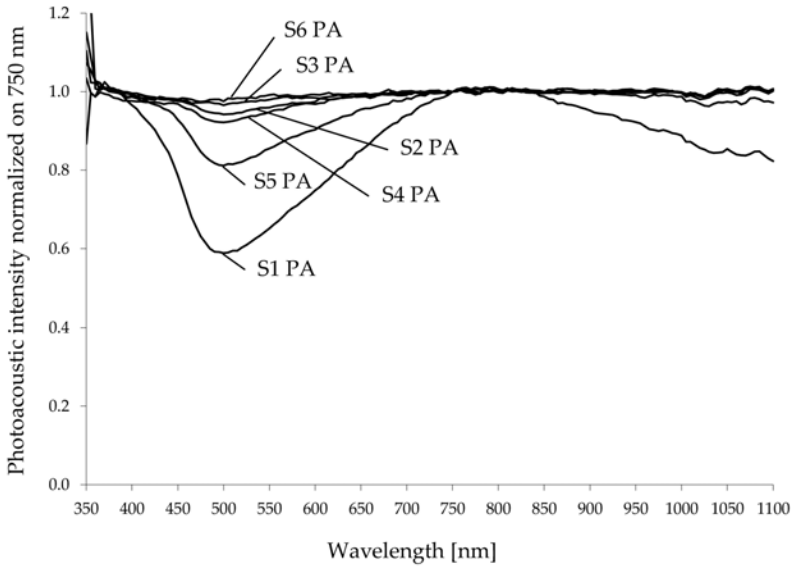

Fig. 3 Normalized photoacoustic spectra at the modulation frequency of 8.5 Hz

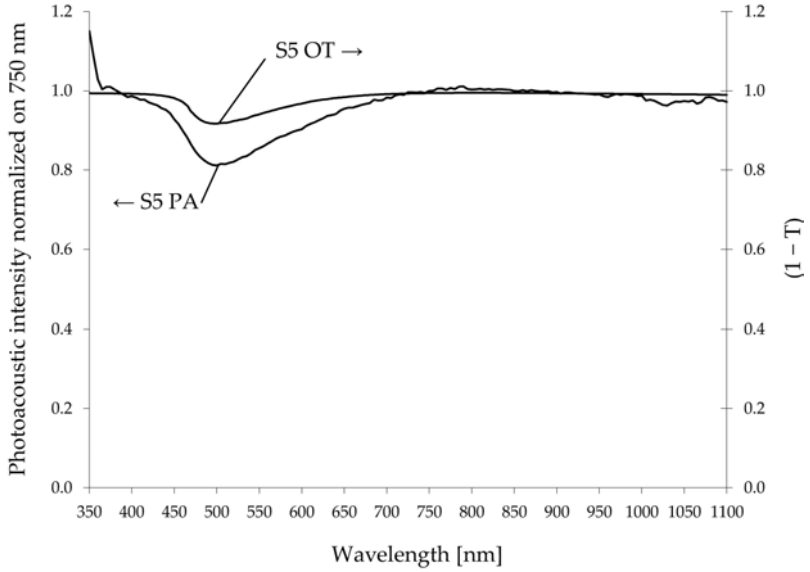

Fig. 4 Comparison of optical transmission (OT) spectrum with normalized photoacoustic (PA) spectrum at the modulation frequency of 8.5 Hz for sample S5

increases with the sample thickness, and the spectra of the samples S3 and S6 are almost fully saturated (the photoacoustic signal is only slightly dependent on the wavelength of the excitation). The possible solution would be to sufficiently increase the modulation frequency [17]. Assuming thermal diffusivity in the order of 10^{-7} m² s^{-1}, common for polymer materials, the thermal diffusion length at 8.5 Hz ranges to tens of micrometres, reaching deep bellow the thickness of all studied samples (thermally thin regime). To limit the measurement to the contribution of a thin surface layer of the sample (thermally thick regime), the thermal diffusion length would have to be sufficiently decreased by measuring at least in the order

of kHz. In current experimental setup, it is not feasible to achieve the sufficient S/N ratio at kHz modulation frequencies. However, compared to the optical transmission spectroscopy, the sensitivity of the photoacoustic spectroscopy is higher even in the thermally thin regime, as illustrates Fig. 4.

The positions of peaks in both the optical transmission and photoacoustic spectra correspond to the conducting form of polyaniline salt. In the work comparing thin polyaniline films obtained by precipitation and dispersion polymerization as an emeraldine salt with corresponding films deprotonated in alkaline media to an emeraldine base [18], a peak with a maximum between 320 and 350 nm due to the π–π* transition was present in the UV–VIS absorption spectra of all four samples. A shoulder at 426 nm together with very broad band starting at 500 nm, having a maximum around 850 nm and then slowly decreasing, which are connected with the transitions involving polaron states (charged cation radicals), were observed in the case of both PANI salts. In the spectrum of PANI base prepared by precipitation polymerization and deprotonation, a broad band assigned to the n– π* transition was observed, starting above 400 nm, having a maximum at 609 nm and then symmetrically decreasing. The spectrum of alkaline media treated PANI dispersion film was closer to the spectrum of PANI salt (in VIS contained the band at 700 nm with a shoulder at 440 nm), indicating higher resistance to deprotonation. All spectra of printed samples of PANI-based dispersion measured by the optical transmission and photoacoustic spectroscopy

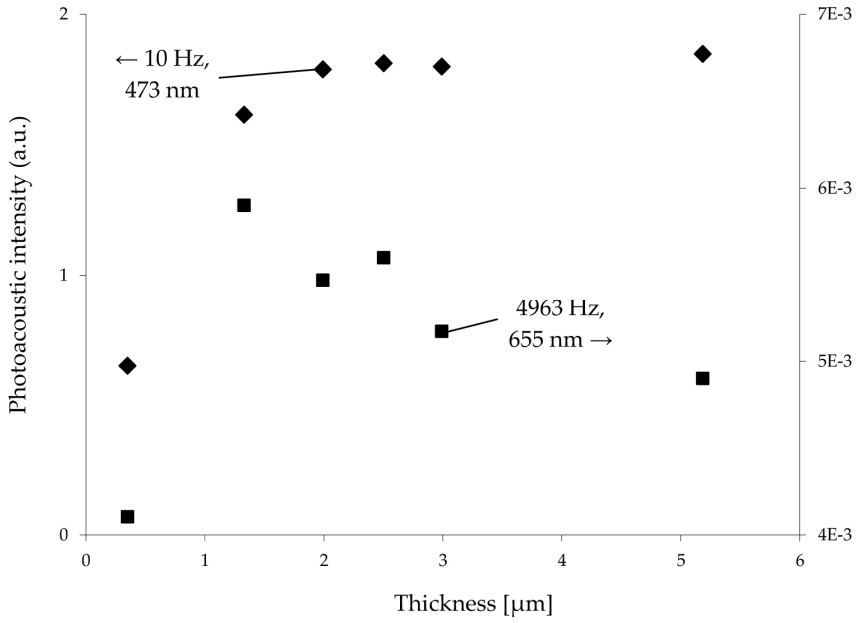

Fig. 5 Correlation between the intensity of the photoacoustic signal at the modulation frequency of 10 Hz and wavelength of 473 nm (diamonds) and at the modulation frequency of 4963 Hz and wavelength of 655 nm (squares), and the sample thickness

within the present study show a minimum around 500 nm. According to the photoacoustic spectra (Fig. 3), the broad band has a maximum at 790 nm and then slowly decreases; going bellow 500 nm, the increase in absorption can be observed as well. The spectra are thus close to those published for conducting emeraldine salt. At the same time, neither the minimum around 400 nm nor the maximum around 600 nm, typical for non-conducting PANI base, are present.

Photoacoustic Depth-Profiling

Similarly to the optical transmission and photoacoustic spectra, the photoacoustics in the modulation frequency domain shows saturation in the intensity of the signal. For the lowest modulation frequencies and the excitation at 473 nm, where the optical absorption is lower, full saturation appears for thickness above 2 μm (diamonds in Fig. 5); at 655 nm it is already above 1 μm. With increasing the modulation frequency, the course of the curves measured for individual printed samples of PANI-based dispersion starts to slightly differ. For the highest measured modulation frequency close to 5 kHz, the intensity of the photoacoustic signal shows small decrease with the thickness except the lowest one (squares in Fig. 5). Nevertheless, for highly absorbing layers with thicknesses in several micrometres, the resolution in the photoacoustic intensity is generally small [17,19]; therefore, better results were expected in the case of the phase of the photoacoustic signal. As illustrates Fig. 6, the changes in the phase induced by different preparation conditions are clearly visible, thus allowing to detect corres-

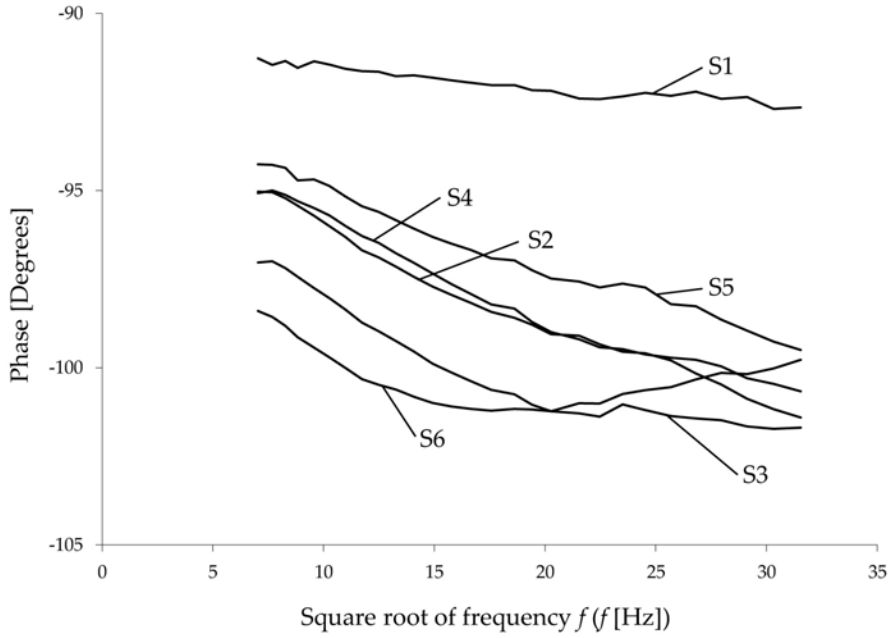

Fig. 6 Modulation frequency dependence of the phase of the photoacoustic signal at the wavelength of 473 nm

ponding variations of printed samples of PANI-based dispersion. Further, the character of the curve measured for the best conducting sample S6 differs from the others. Since besides the sample thickness, the photoacoustic signal depends on the optical and thermal properties within its depth [20], the throughout interpretation of the results would need more detailed study on higher number of samples with varying parameters, leading to the estimation of the optical and thermal parameters of both individual components and resulting non-homogeneous layers.

Conclusion

It was confirmed that the PANI/PVP water based colloidal dispersion can be applied by means of the screen printing and that the properties of printed layers can be influenced by modification of printing formulation and parameters. The prepared screen printed PANI/PVP samples were conducting (up to 7.5 mS cm^{-1}) and their conductivity corresponds to typical semiconductors. The thickness of PANI/PVP layers was a few micrometres, with the surface roughness not exceeding 1 μm. The prepared samples, however, were not fully homogenous and contained aggregates and pinholes; therefore, the quality of the printed layers still needs to be improved by tuning the ink formulation. Furthermore, based on the correlation of values of roughness and thickness and its comparison with specific conductivity, dividing the samples into two groups (S1, S3 and S5 as the first and S2, S4 and S6 as the second), there seems to be a relationship between the roughness and specific conductivity. To confirm or disprove this observation, the investigation on a considerably larger set of samples is needed.

The prepared PANI/PVP layers were characterized by means of the image analysis based on fractal spectra and the photoacoustics and photoacoustic spectroscopy. It was shown, that defects and changes in the structure and properties of the layers can be detected and qualitatively evaluated. With the optimization of the experimental setup, the quantitative evaluation should be possible. Accordingly, these characterization methods could be later potentially used for the inline assessment in the production lines.

Acknowledgement

The authors thank the Technology Agency of the Czech Republic (TE01020022) for financial support.

References

[1] Sekitani T., Someya T.: Adv. Mater. **22**, 2228 (2010).
[2] Jung S., Sou A., Gili E., Sirringhaus H.: Org. Electron. **14**, 699 (2013).
[3] Morvillo P., Grimaldi I., Diana R., Loffredo F., Villani F.: J. Mater. Sci. **48**, 2920 (2013).
[4] Gomes T.C., Constantino C.J.L., Lopes E.M., Job A.E., Alves N.: Thin Solid Films **520**, 7200 (2012).
[5] Kit-Anan W., Olarnwanich A., Sriprachuabwong C., Karuwan C., Tuantranont A., Wisitsoraat A., Srituravanich W., Pimpin A.: J. Electroanal. Chem. **685**, 72 (2012).
[6] Kulkarni M.V., Charhate N.A., Bhavsar K.V., Tathe M.A., Kale B.B.: Mater. Res. Innov. **17**, 238 (2013).
[7] Wang S.S., Lu S., Su J., Guo Z.K., Li X.M., Zhang X.H., He T.: Acta Phys.-Chim. Sinica **29**, 516 (2013).
[8] Molberg M., Crespy D., Rupper P., Nüesch F., Månson J.-A.E., Löwe C., Opris D.M.: Adv. Funct. Mater. **20**, 3280 (2010).
[9] Liang Y., Tao Z., Chen J.: Adv. Energy Mater. **2**, 742 (2012).
[10] Ihalainen P., Määttänen A., Mattinen U., Stępień M., Bollström R., Toivakka M., Bobacka J., Peltonen J.: Thin Solid Films **519**, 2172 (2011).
[11] Yussuf A.A., Sbarski I., Solomon M., Tran N., Hayes J.P.: J. Mater. Process. Technol. **189**, 401 (2007).
[12] Stejskal J., Sapurina I.: Pure Appl. Chem. **77**, 815 (2005).
[13] Peřinka N., Kaplanová M., Syrový T., Exnerová M., Stejskal J.: Chem. Listy **106**, 1338 (2012).
[14] Zmeškal O., Buchníček M., Nežádal M.: Image Science Fundamentals. Available [online] http://www.fch.vutbr.cz/lectures/imagesci/ [28Jun2010].
[15] Holická H., Držková M.: TAPPI J. **11**, 21 (2012).
[16] Zmeškal O., Nežádal M., Buchníček M.: J. Im. Sci. Tech. **46**, 453 (2002).
[17] Rosencwaig A.: *Photoacoustics and Photoacoustic Spectroscopy, Chemical Analysis V57*, pp 106-107, John Wiley & Sons, New York, 1980.
[18] Rozlívková Z., Trchová M., Šeděnková I., Špírková M., Stejskal J.: Thin Solid Films **519**, 5933 (2011).
[19] Peřinka N., Syrová L., Držková M., Syrový T., Kaplanová M.: *Photoacoustic Measurement of Screen-Printed Conductive Layers*, in: *Advances in Printing and Media Technology*, Vol. XXXIX (N. Enlund, M. Lovreček, Eds.), pp 17-22, International Association of Research Organizations for the Information, Media and Graphic Arts Industries, Darmstadt, 2012.
[20] Hu H., Wang X., Xu X.: J. Appl. Phys. **86**, 3953 (1999).